Two-polaron energy diffusion in a one-dimensional lattice of hydrogen bounded peptide units

Vincent J.C. Pouthier

Two-polaron energy diffusion in a one-dimensional lattice of hydrogen bounded peptide units

V. Pouthier

Laboratoire de Physique Moléculaire, UMR CNRS 6624, Université de Franche-Comté, 25030 Besançon cedex - France

E-mail: vincent.pouthier@univ-fcomte.fr

Abstract. A generalized Pauli master equation is established for describing the vibrational energy flow in a 1D lattice of hydrogen bounded peptide units. A Lang-Firsov transformation is applied so that the relevant excitations are small polarons corresponding to vibrational excitons dressed by virtual phonons. A special attention is thus paid to characterize the energy transfer mediated by two polarons. At biological temperature, it is shown that the polaron-phonon coupling is sufficiently strong to prevent any coherent motion. The polaron-polaron interaction occurring in such a nonlinear lattice does not affect the long time behavior of the energy flow which results from the diffusion of two independent polarons. This diffusive motion originates in the competition between two contributions related to phonon mediated transitions (incoherent contribution) and to dephasing limited coherent motion (coherent contribution).

PACS numbers: 05.60.Gg,63.20.Ls,71.38.Ht,87.14.Ee

Keywords: Nonlinear lattice, proteins, bi-polaron, energy diffusion

1. Introduction

In the 70th, Davydov and co-workers [1] have developed a soliton formalism to explain how the energy released by the hydrolysis of adenosine triphophate (ATP) can be transported in α-helices. The main idea is that the released energy, stored in the high-frequency amide-I vibration of a peptide group, delocalizes along the helix leading to the formation of vibrational excitons called vibrons. Their interaction with the phonons of the helix induces a nonlinear dynamics which counterbalances the dispersion. It yields the creation of the so called Davydov's soliton which is the solution of the Nonlinear Schrodinger (NLS) equation within the continuum approximation [2, 3]. Moreover, the discrete version of NLS yields the occurrence of discrete breathers which correspond to time-periodic and spatially localized solutions [4, 5, 6]. Contrary to solitons, they do not require integrability for their existence and stability and they correspond to quite general and robust solutions [7].

Although this formalism gives a comprehensive schema for explaining energy transport in living systems, no clear evidence has yet been found for the existence of solitons in real proteins. Therefore, it has been suggested that the solution is a small polaron formed by a vibron dressed by a virtual cloud of phonons [8, 9, 10, 11, 12].

Recently, the polaron approach has been improved to characterize the two-polaron energy spectrum with a special emphasis onto the interplay between the dressing effect and the intramolecular anharmonicity of each amide-I vibration [13, 14, 15, 16, 17]. Both features favor the formation of two-polaron bound states (TPBS) which correspond to the trapping of the two quanta over only a few neighboring peptide groups with a resulting energy which is lesser than the energy of two quanta lying far apart. The separating distance between the two quanta is localized so that they behave as a single particle delocalized along the lattice and they can be viewed as the quantum counterpart of breathers or solitons [18, 19, 20, 21, 22, 23]. In fact, the helix supports two kinds of bound states referring to the trapping of two polarons onto the same amide-I mode (TPBS-I) and onto two nearest neighbor amide-I vibrations (TPBS-II). These results were corroborated by a recent experiment devoted to the femtosecond infrared pump-probe spectroscopy of the N-H mode in a stable α-helix which has revealed the two excited state absorption bands connected to the two kinds of bound states [24].

Within the polaron formalism, the strong vibron-phonon interaction is partially removed so that a polaron-phonon coupling remains. This coupling has been considered in a previous work to characterize the relaxation mechanisms [14]. It has been shown that it is responsible for the occurrence of transitions between two-polaron eigenstates mediated by both phonon absorption and phonon emission. At biological temperature, we have established that the relaxation rate does not depends significantly on the nature of the two-polaron states involved in the process. By contrast, the relaxation channels strongly depend on the nature of the two-polaron states since TPBS-I tend to decay into TPBS-II whereas TPBS-II decay into both TPBS-I and the continuum of two-polaron free states (TPFS).

Nevertheless, the calculation of the relaxation rates is not sufficient to reach a complete understanding of the diffusion of two trapped polarons and a more general approach is needed. This is the goal of the present paper in which the vibrational energy diffusion mediated by two polarons is addressed through the generalization of the kinetic method used to study the diffusion of a single particle (see for instance Refs. [25, 26, 27, 28, 29] and references therein).

The paper is organized as follows. In Section 2, the Davydov model is first described and the small polaron point of view is established. Then, the nature of the two-polaron quantum eigenstates are summarized. In Section 3, the key observables required to study the transport properties are introduced. In Section 4, the polaron-phonon coupling is treated and a quantum kinetic equation for the polaron reduced density matrix is established. The generalized Pauli master equation is defined in Section 5. This equation is solved numerically in Section 6 where a detailed analysis of the transport properties is performed. Finally, these results are discussed and interpreted in Section 7.

2. Description of the system

2.1. Model and Hamiltonians

According to the Davydov model, the vibron-phonon dynamics in an α-helix is described by a 1D lattice of hydrogen bounded peptide units formed by N sites. Each site is occupied by a peptide group which contains the amide-I vibration. The nth amide-I vibration behaves as a high frequency anharmonic oscillator described by the creation and annihilation vibron operators b_n^+ and b_n. The vibron Hamiltonian is thus written as (using the convention $\hbar$=1)

$$H_v = \sum_n \omega_0 b_n^\dagger b_n - A b_n^\dagger b_n^\dagger b_n b_n - \sum_n J[b_n^\dagger b_{n+1} + b_{n+1}^\dagger b_n] \tag{1}$$

where ω_0 is the internal frequency of each amide-I mode, A is the intramolecular anharmonicity and J denotes the vibron hopping constant.

The amide-I vibrations interact with the phonons of the lattice which characterize the external motions of the peptide groups. They correspond to a set of N acoustic modes, labeled $\{q\}$, whose Hamiltonian is defined as

$$H_p = \sum_q \Omega_q a_q^\dagger a_q \tag{2}$$

where $a_q^\dagger$ and a_q are the phonon operators of the qth mode with frequency $\Omega_q = \Omega_c \mid \sin(q/2) \mid$, Ω_c denoting the phonon cutoff frequency.

Finally, the vibron-phonon interaction Hamiltonian characterizes a random modulation of the internal frequency of each amide-I mode as

$$\Delta H_{vp} = \sum_{qn} (\Delta_{qn} a_q^\dagger + \Delta_{qn}^* a_q) b_n^\dagger b_n \tag{3}$$

where the coupling constant $\Delta_{qn} = -i\frac{\Delta_0}{\sqrt{N}} \sin(q)/\sqrt{|\sin(q/2)|} e^{-iqn}$ is expressed in terms of the strength of the vibron-phonon coupling Δ_0.

To partially remove the vibron-phonon coupling, the small polaron point of view has been used in several previous works. Here, we give a brief summary of the procedure and a detailed analysis can be found in Refs [11, 12, 13, 14, 15, 16, 17]. To proceed, a Lang-Firsov transformation [30] is applied so that the transformed Hamiltonian is written as

$$\begin{aligned}\hat{H} = & \sum_n \hat{\omega}_0 b_n^\dagger b_n - \hat{A} b_n^{\dagger 2} b_n^2 - E_B b_{n+1}^\dagger b_{n+1} b_n^\dagger b_n \\ & - \sum_n J(\Theta_{n+1}^\dagger \Theta_n b_{n+1}^\dagger b_n + \Theta_n^\dagger \Theta_{n+1} b_n^\dagger b_{n+1}) + H_p \end{aligned} \tag{4}$$

where $\hat{\omega}_0 = \omega_0 - E_B$ and $\hat{A} = A + E_B$ are expressed in terms of the small polaron binding energy $E_B = 2\Delta_0^2/\Omega_c$ and where Θ_n stands for the dressing operator defined as

$$\Theta_n = \exp[-\sum_{qn}(\frac{\Delta_{qn}}{\Omega_q} a_q^\dagger - \frac{\Delta_{qn}^*}{\Omega_q} a_q)] \tag{5}$$

The next step of the procedure consists in expressing $\hat{H}$ as the sum of three separated contributions as $\hat{H} = H_{po} + H_p + \Delta H$. The polaron Hamiltonian H_{po}, obtained after performing a thermal average over the phonon degrees of freedom, is written as

$$\begin{aligned} H_{po} = & \sum_n \hat{\omega}_0 b_n^\dagger b_n - \hat{A} b_n^\dagger b_n^\dagger b_n b_n - E_B b_{n+1}^\dagger b_{n+1} b_n^\dagger b_n \\ & - \hat{J}(b_{n+1}^\dagger b_n + b_n^\dagger b_{n+1}) \end{aligned} \tag{6}$$

where the effective hopping constant $\hat{J} = J\exp(-S(T))$ is expressed in terms of the coupling constant $S(T)$ defined as

$$S(T) = \sum_q \frac{4E_B}{N\Omega_c} \mid \sin(\frac{q}{2}) \mid \cos^2(\frac{q}{2}) \coth(\frac{\Omega_q}{2k_B T}) \tag{7}$$

Finally, the remaining part of the polaron-phonon interaction ΔH is defined as

$$\Delta H = \sum_n V_{n+1,n} b_{n+1}^\dagger b_n + V_{n,n+1} b_n^\dagger b_{n+1} \tag{8}$$

where $V_{n,n'} = \hat{J} - J\Theta_n^\dagger \Theta_{n'}$

In this new point of view, the operators $b_n^\dagger$ and b_n define small polarons corresponding to vibrons dressed by a lattice distortion. The dressing prevents the delocalization of the polarons whose effective hopping constant $\hat{J}$ is smaller than the bare constant J. It yields a redshift of the vibrational frequency of each mode and produces additional anharmonicities characterizing the interaction between polarons due to the overlap between their virtual cloud of phonons. Finally, the polaron-phonon coupling remains through the modulation of the lateral term by the dressing operator fluctuations. Although these operators depend on the phonon coordinates in a highly nonlinear way, the interaction has been strongly reduced and a standard perturbation theory can be applied. This procedure requires the knowledge of the properties of the unperturbed polarons which are summarized in the next section.

2.2. Two-polaron eigenstates

As detailed in Ref. [13], the Schrodinger equation $H_{po} \mid \Psi\rangle = \omega \mid \Psi\rangle$ has to be solved to characterize the entire two-polaron energy spectrum. This can be achieved by using the number states method [22] in which the two-polaron wave function is expanded as

$$|\Psi\rangle = \sum_{x_1,x_2} \Psi(x_1,x_2)|x_1,x_2) \tag{9}$$

where $\{|x_1,x_2)\}$ is a local basis set normalized and symmetrized according to the restricting $x_2 \geq x_1$ and where a vector $|x_1,x_2)$ characterizes two polarons located onto the sites x_1 and x_2, respectively. This basis set generates the entire two-polaron subspace $\mathcal{E}_2$ whose dimension $N(N+1)/2$ represents the number of ways for distributing two indistinguishable quanta onto N sites.

By taking advantage of the lattice periodicity, the wave function is expanded as a Bloch wave as

$$\Psi(x_1, x_2 = x_1 + m_x) = \frac{1}{\sqrt{N}} \sum_{x_1} e^{ik(x_1+m_x/2)} \Psi_k(m_x) \tag{10}$$

where the total momentum k is associated to the motion of the polaron center of mass and where the wave function $\Psi_k(m_x)$ characterizes the polaron inter-distance m_x. Since k is a good quantum number, H_{po} is block diagonal and the Schrodinger equation can be solved for each k value. For a given k value, the lattice exhibits two different eigenstates, i.e. TPFS and TPBS. The TPFS correspond to a delocalization of the inter-distance m_x. The wave function $\Psi_k(m_x)$ behaves as a plane wave and the TPFS belong to an energy continuum. By contrast, the TPBS correspond to a localization of the inter-distance and characterize the trapping of the two quanta over only a few neighboring sites. We have shown that the α-helix supports two kinds of bound states, called TPBS-I and TPBS-II, respectively. The TPBS-I are low frequency bound states located below the TPFS continuum over the entire Brillouin. For TPBS-II, two situations occur depending on the strength of the small polaron binding energy. For small E_B values, the band shows a resonance with the continuum whereas, for strong E_B values, the band is located below the continuum. In the harmonic situation, TPBS-I and TPBS-II are combinations of states involving the trapping of the two polarons onto the same amide-I mode and onto nearest neighbor amide-I modes. By contrast, the intramolecular anharmonicity reduces the hybridization and TPBS-I refer to the trapping of the two polarons onto the same amide-I mode whereas TPBS-II characterize the trapping onto nearest neighbor amide-I vibrations.

At this step, let us mention that the local basis set $\{|x_1,x_2)\}$ yields an equivalence between the two-polaron dynamics and the motion of a single particle on the 2D lattice displayed in Fig. 1. Indeed, x_1 and x_2 can be viewed as the coordinates of the vector $\mathbf{x}$ which specifies the position of the fictitious particle. Note that to account for this feature we introduce the notation $|\mathbf{x})$ to define the basis vector $|x_1,x_2)$. Within this equivalence, $\Psi(x_1,x_2)$ corresponds to the wave function of the particle whose dynamics is governed by a tight-binding Hamiltonian. Each site $\mathbf{x}$ of the 2D equivalent lattice

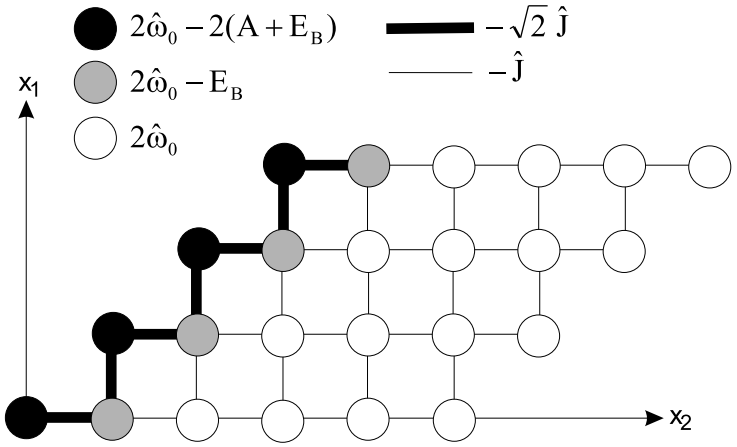

Figure 1. Equivalence between the two-polaron dynamics and the tight binding model for a single fictitious particle moving on a 2D lattice.

is characterized by the self-energy $\epsilon_{\mathbf{x}} = 2\hat{\omega}_0$ and nearest neighbor sites are coupled through the hopping constant $\hat{J}$. However, the 2D lattice exhibits two rows of defects which yield a redshift of the self-energies and a modification of the hopping constants. When $x_2 = x_1$, the two polarons are located on the same site so that the self-energy is equal to $\epsilon_{\mathbf{x}} = 2\hat{\omega}_0 - 2\hat{A}$. In the same way, when $x_2 = x_1 + 1$, the polarons occupy nearest neighbor sites and the corresponding self-energy is equal to $\epsilon_{\mathbf{x}} = 2\hat{\omega}_0 - E_B$. Therefore, such defects discriminate between two different eigenstates. The eigenstates of the core of the lattice describe plane waves slightly perturbed by the defects and correspond to the TPFS. By contrast, the presence of the defects leads to the occurrence of localized states which are associated to the TPBS.

3. Transport properties

Without any perturbation, the system is in thermal equilibrium at a temperature T at least equal to the room temperature. Since the relation $\hbar\omega_0 >> k_B T$ is fulfilled whatever T (k_B is the Boltzmann constant), only the ground state with zero vibron is significantly populated. This is no longer the case for the acoustic phonons ($\Omega_c << \omega_0$) assumed to be in thermal equilibrium and described by the Boltzmann distribution ρ_p.

To study the vibrational energy diffusion we suppose that two vibrons are initially created on the site $n = x_0$ so that the lattice reaches a configuration out of equilibrium. Since the coupling with the phonon bath Eq.(3) conserves the vibron number, it accounts for dephasing mechanism only and does not allow for energy relaxation. Therefore, the diffusion characterizes the return to a quasi-equilibrium in which the vibron number is equal to two. The processes involved to reach the thermal equilibrium are assumed to take place over a timescale several orders of magnitude greater than the dephasing time and they will be disregarded in the present work. Therefore, the initial density matrix for the whole system can be written as the tensorial product $\rho = \rho_v \otimes \rho_p$ where

$\rho_v = |\mathbf{x}_0)(\mathbf{x}_0|$.

To characterize the vibrational energy flow, we introduce the vibron density $g_n(t) = \langle b_n^\dagger(t) b_n(t) \rangle$ which represents the average value of the number of quanta on the nth site at time t. Since the vibron number is conserved under the Lang-Firsov transformation, the vibron population is equal to the polaron population. As a consequence, in the polaron point of view, the time evolution is given by the Heisenberg representation with respect to the full Hamiltonian $\hat{H}$ (Eq.(4)) and the vibron density is expressed as

$$g_n(t) = Tr[\hat{\rho} e^{i\hat{H}t} b_n^\dagger b_n e^{-i\hat{H}t}] \tag{11}$$

where $\hat{\rho}$ is the transformed initial density matrix. The polaron density matrix is equivalent to the vibron density matrix whereas the phonon density matrix is modified since the creation of two vibrons yields two polarons accompanied by a local disturbance of the phonon state. Nevertheless, in the following of the paper it will be assumed that the lattice is fully relaxed before the two polarons begin to move [31]. This feature allows us to neglect the modification of the phonon density matrix so that $\hat{\rho} \approx \rho_v \otimes \rho_p$.

Within the local basis set, the population operator is diagonal ($(\mathbf{x}|b_n^\dagger b_n|\bar{\mathbf{x}}) = \delta_{\mathbf{x},\bar{\mathbf{x}}}(\delta_{n,x_1} + \delta_{n,x_2})$) so that the vibron density is expressed as

$$g_n(t) = \sum_{\mathbf{x}} (\mathbf{x}|b_n^\dagger b_n|\mathbf{x}) \sigma(\mathbf{x}, \mathbf{x}, t) \tag{12}$$

where $\sigma(\mathbf{x}, \mathbf{y}, t)$ denotes the time dependent reduced density matrix defined as

$$\sigma(\mathbf{x}, \mathbf{y}, t) = \mathrm{Tr}[|\mathbf{x}_0)(\mathbf{x}_0|\rho_p e^{i\hat{H}t}|\mathbf{y})(\mathbf{x}|e^{i\hat{H}t}] \tag{13}$$

The reduced density matrix describes the two-polaron states at time t after performing the average over the phonon degrees of freedom. It is the central object of the present study whose knowledge allows us to compute in principle all the required observables to describe the energy flow. Therefore, the following section is devoted to the derivation of a quantum kinetic equation to study its time evolution.

4. Quantum kinetic equation

4.1. General expression

To characterize the time evolution of the reduced density matrix let us introduce the Liouville space formalism described in details in Ref. [32]. When two polarons are excited, the Liouville space is defined as the tensorial product $\mathcal{L}_2 = \mathcal{E}_2 \otimes \mathcal{E}_2^\dagger$. A useful basis set to generate $\mathcal{L}_2$ is formed by the vectors $|\mathbf{x}, \mathbf{y}^\dagger\rangle\rangle$, which correspond to the operators $|\mathbf{x})(\mathbf{y}|$, so that $\sigma(\mathbf{x}, \mathbf{y}, t)$ is the projection of a vector $|\sigma(t)\rangle\rangle$. Therefore, since the total trace in Eq.(13) can be splitted into partial traces over the polaron and phonon degrees of freedom, the reduced density matrix is rewritten as

$$\sigma(\mathbf{x}, \mathbf{y}, t) = \langle\langle \mathbf{x}_0^\dagger, \mathbf{x}_0| \, \mathrm{Tr}_p \, \rho_p e^{i\hat{L}t} |\mathbf{y}, \mathbf{x}^\dagger\rangle\rangle \tag{14}$$

where $\hat{L} = [\hat{H}, ...]$ is the Liouvillian associated to the full Hamiltonian.

To determine the time evolution of the reduced density matrix, we use the Zwanzig-Mori's projector technique [32, 33, 34] which has demonstrated its usefulness in eliminating irrelevant information from a system and extracting only the information that is desired. By performing a second order perturbation theory with respect to ΔH (Eq. (8)), it is straightforward to show that the reduced density matrix satisfies the kinetic equation

$$\frac{\partial|\sigma(t)\rangle\rangle}{\partial t} = -iL_{po}|\sigma(t)\rangle\rangle - \int_0^t d\tau J(\tau)|\sigma(t-\tau)\rangle\rangle \tag{15}$$

where $L_{po} = [H_{po}, ...]$ and where the kernel memory $J(t)$ is a superoperator whose elements are defined as

$$\begin{aligned}\langle\langle \mathbf{x}^\dagger, \mathbf{y}|J(t)|\bar{\mathbf{x}}, \bar{\mathbf{y}}^\dagger\rangle\rangle = & \ \mathrm{Tr}_p\, \rho_p(\bar{\mathbf{y}}|\Delta H(0)G^\dagger(t)\Delta H(t)|\mathbf{y})(\mathbf{x}|G(t)|\bar{\mathbf{x}}) \\ & + \ \mathrm{Tr}_p\, \rho_p(\bar{\mathbf{y}}|G^\dagger(t)|\mathbf{y})(\mathbf{x}|\Delta H(t)G(t)\Delta H(0)|\bar{\mathbf{x}}) \\ & - \ \mathrm{Tr}_p\, \rho_p(\bar{\mathbf{y}}|\Delta H(0)G^\dagger(t)|\mathbf{y})(\mathbf{x}|\Delta H(t)G(t)|\bar{\mathbf{x}}) \\ & - \ \mathrm{Tr}_p\, \rho_p(\bar{\mathbf{y}}|G^\dagger(t)\Delta H(t)|\mathbf{y})(\mathbf{x}|G(t)\Delta H(0)|\bar{\mathbf{x}})\end{aligned} \tag{16}$$

In Eq.(16), the time dependence of ΔH results from an Heisenberg representation with respect to the phonon Hamiltonian and $G(t) = \exp(-iH_{po}t)$ is the two-polaron evolution operator.

The first term in the right-hand-side of Eq.(15) characterizes the coherent dynamics of the unperturbed polarons. It corresponds to the free evolution of the reduced density matrix under the influence of the polaron Hamiltonian H_{po}. By contrast, the kernel memory Eq.(16) represents the relaxation mechanisms. It accounts for the modification of the dynamics of the reduced density matrix at time t due to the history of the polaron-phonon coupling between $t = 0$ and t.

4.2. Approximate kinetic equation

As shown in Eq. (16), the kernel memory is expressed in terms of the correlation functions of the polaron-phonon coupling Hamiltonian. These correlation functions are characterized by the correlation time τ_c of the phonon bath which measures the time for which the correlations vanish. In a general way, τ_c is very short when compared with the typical time governing the free evolution of the reduced density matrix [17]. As a consequence, this assumption allows us to invoke three simplifying approximations. First, we assume that over a timescale of about τ_c, a polaron does not have enough time to realize a transition between two lattice sites. In the local basis, the non diagonal elements of the free propagator $G(t)$ can thus be neglected in Eq.(16). Then, the Markovian limit of the kinetic equation is assumed to be reached. Finally, we suppose that the phonon bath cannot develop spatial correlations. The only non vanishing correlation functions of the polaron-phonon coupling Hamiltonian thus involve the following auto-correlations (see Eq.(8))

$$C(t) = \mathrm{Tr}_p[\rho_p V_{n,n\pm1}(t)V_{n\pm1,n}(0)] \tag{17}$$

Therefore, after performing some algebraic calculations, these assumptions yield an approximate quantum kinetic equation as

$$\frac{\partial|\sigma(t)\rangle\rangle}{\partial t} = -iL_{po}|\sigma(t)\rangle\rangle - (\hat{\Gamma} + \hat{W})|\sigma(t)\rangle\rangle \tag{18}$$

where the non vanishing matrix elements of the superoperators $\hat{\Gamma}$ and $\hat{W}$ are defined as

$$\begin{aligned}
&\langle\langle \mathbf{x}^\dagger, \mathbf{y}|\Gamma|\mathbf{x}, \mathbf{y}^\dagger\rangle\rangle = (1 - \delta_{\mathbf{x},\mathbf{y}})\Gamma_{\mathbf{x},\mathbf{y}} \\
&\langle\langle \mathbf{x}^\dagger, \mathbf{x}|\hat{W}|\bar{\mathbf{x}}, \bar{\mathbf{x}}^\dagger\rangle\rangle = [\delta_{\mathbf{x},\bar{\mathbf{x}}} \sum_{\mathbf{x}'} W^i_{\mathbf{x}\to\mathbf{x}'} - (1 - \delta_{\mathbf{x},\bar{\mathbf{x}}})W^i_{\bar{\mathbf{x}}\to\mathbf{x}}]
\end{aligned} \tag{19}$$

In Eq.(19), the dephasing constant $\Gamma_{\mathbf{x},\mathbf{y}}$ is written as

$$\begin{aligned}
\Gamma_{\mathbf{x},\mathbf{y}} = &\int_0^{+\infty} 2C(t)G^*(m_y, t)[(1 + \delta_{m_x,0})G(m_x + 1, t) \\
&+ (1 + \delta_{m_x,1})G(m_x - 1, t)]dt \\
&+ \int_0^{+\infty} 2C^*(t)G(m_x, t)[(1 + \delta_{m_y,0})G^*(m_y + 1, t) \\
&+ (1 + \delta_{m_y,1})G^*(m_y - 1, t)]dt
\end{aligned} \tag{20}$$

Similarly, rate $W^i_{\mathbf{x}\to\bar{\mathbf{x}}}$, which connects nearest neighbor basis vectors $|\mathbf{x})$ and $|\bar{\mathbf{x}})$ in the 2D equivalent lattice shown in Fig. 1, is expressed as

$$\begin{aligned}
W^i_{\mathbf{x}\to\bar{\mathbf{x}}} = 2\Re \int_0^{+\infty} &dtC(t)(1 + \delta_{m_x,0})(1 + \delta_{m_{\bar{x}},0}) \\
&G^*(m_x, t)G(m_{\bar{x}}, t)
\end{aligned} \tag{21}$$

Note that $G(m_x, t) = (\mathbf{x}|G(t)|\mathbf{x})$ is the diagonal element of the two-polaron evolution operator which only depends on the inter-distance $m_x = x_2 - x_1$.

Besides the coherent term, the kinetic equation Eq.(18) contains two contributions characterizing irreversible processes which originate from the coupling between the polarons and the phonon bath. The first term, proportional to the dephasing constant $\Gamma_{\mathbf{x},\mathbf{y}}$, shows how the dephasing limits the coherent motion of the polarons. The second term appears as a Pauli master equation for the diagonal elements of the reduced density matrix and involves the transition rates $W^i_{\mathbf{x}\to\bar{\mathbf{x}}}$. Note that the interpretation of the kinetic equation is rather simple within the equivalence between the two-polaron dynamics and the motion of the single particle. Indeed, the coherent motion of the particle leads to its delocalization over the sites of the 2D lattice. Its eigenstate is thus described by a superimposition of the local basis vectors, the phase of which are related to each other when the time evolution is governed by the polaron Hamiltonian, only. However, during this evolution, the coupling with the phonons induces random fluctuations of each phase which destroy the coherence. As a result, the nature of the motion evolves from a coherent to an incoherent one. In addition, the coupling with the phonons favors random fluctuations of the hopping constant between nearest neighbor sites of the 2D lattice. Consequently, the particle realizes incoherent hops between sites mediated by the absorption and the emission of phonons.

5. Pauli Master equation

5.1. General expression

As shown in Eq.(12), the characterization of the vibron density requires the knowledge of the population $P(\mathbf{x},t) = \sigma(\mathbf{x},\mathbf{x},t)$. To extract these populations form the general expression of the density matrix, let us define the projector P on the populations. By applying the well known projector method, the kinetic equation Eq.(18) can be expressed as a system of two coupled equations for the evolution of both $P|\sigma(t)\rangle\rangle$ and $Q|\sigma(t)\rangle\rangle$, where $Q = 1 - P$. Since we have assumed that initially a vibron pair is created on the site x_0, the projection $Q|\sigma(0)\rangle\rangle$ vanishes. Therefore, the system of equations can be solved first by obtaining the formal expression of $Q|\sigma(t)\rangle\rangle$ and then by inserting this expression in the equation connected to the evolution of $P|\sigma(t)\rangle\rangle$. The required kinetic equation for the projection $P|\sigma(t)\rangle\rangle$ is finally written as

$$\begin{aligned}\frac{\partial P|\sigma(t)\rangle\rangle}{\partial t} = & - P\hat{W}P|\sigma(t)\rangle\rangle \\ & - \int_0^t d\tau P L_{po} Q e^{-iQ(L_{po}-i\hat{\Gamma})Q\tau} Q L_{po} P|\sigma(t-\tau)\rangle\rangle \end{aligned} \tag{22}$$

At this step, let us mention that the numerical calculations presented in the following sections will be performed at biological temperature. In that case, for the amide-I vibration, we have verified that the dephasing constant is sufficiently important to prevent almost any coherent motion of the two polarons. In other words, Eq.(22) can be simplified by invoking the Markov approximation, as

$$\frac{\partial P|\sigma(t)\rangle\rangle}{\partial t} = -[P\hat{W}P + PL_{po}Q\frac{1}{Q(\hat{\Gamma}+iL_{po})Q}QL_{po}P]P|\sigma(t)\rangle\rangle \tag{23}$$

By performing a perturbative expansion with respect to the effective hopping constant, the evolution of the populations is finally ruled by a generalized Pauli master equation expressed as

$$\frac{\partial P(\mathbf{x},t)}{\partial t} = \sum_{\bar{\mathbf{x}}} W_{\bar{\mathbf{x}}\to\mathbf{x}} P(\bar{\mathbf{x}},t) - W_{\mathbf{x}\to\bar{\mathbf{x}}} P(\mathbf{x},t) \tag{24}$$

where the full transition rate $W = W^i + W^c$ is expressed in terms of the rate W^c defined as

$$W^c_{\mathbf{x}\to\bar{\mathbf{x}}} = 2\Re\frac{|(\mathbf{x}|H_{po}|\bar{\mathbf{x}})|^2}{\Gamma_{\mathbf{x},\bar{\mathbf{x}}} + i(\epsilon_{\mathbf{x}} - \epsilon_{\bar{\mathbf{x}}})} \tag{25}$$

Eq.(24) is a standard Pauli master equation which governs the time evolution of the population of the local basis vectors. This equation involves two kinds of transition rates. As in Eq.(18), the rate $W^i_{\mathbf{x}\to\bar{\mathbf{x}}}$ characterizes an incoherent transition between two nearest neighbor local basis vectors mediated by the exchange of phonons. By contrast, the rate $W^c_{\mathbf{x}\to\bar{\mathbf{x}}}$ describes how the dephasing limits the coherent motion of the polarons. It defines transitions between the different states $|\mathbf{x})$ which result from the ability of the polaron Hamiltonian to produce quantum states as coherent superimpositions of the

local basis vectors. However, dephasing tends to destroy such superimpositions so that the resulting process is a hop between two local basis vectors. For that reason, this rate will be called the coherent rate.

5.2. Bloch transformation and Observables

As shown in Eq.(21), the rate $W^i_{\mathbf{x}\to\bar{\mathbf{x}}}$ describes an incoherent transition between two nearest neighbor basis vectors $|\mathbf{x}) \equiv |x_1, x_1 + m_x)$ and $|\bar{\mathbf{x}}) \equiv |\bar{x}_1, \bar{x}_1 + m_{\bar{x}})$. This rate only depends on m_x and $m_{\bar{x}}$ so that it respects the translational invariance of the 2D equivalent lattice displayed in Fig. 1. In others words, this rate does not depends on the position of the center of mass of the two polarons but only depends on the separating distance between them. This fundamental remark is also valid for both the dephasing constant $\Gamma_{\mathbf{x},\mathbf{y}}$ and the coherent rate $W^c_{\mathbf{x}\to\bar{\mathbf{x}}}$. As a consequence, the notations can be simplified as

$$\begin{aligned} W_{\mathbf{x}\to\bar{\mathbf{x}}} &\equiv W_{m_x\to m_{\bar{x}}} \\ \Gamma_{\mathbf{x},\mathbf{y}} \quad &\equiv \Gamma_{m_x,m_y} \end{aligned} \tag{26}$$

In that context, the Pauli master equation Eq.(24) can be expressed in an improved way by taking advantage of the lattice periodicity. Indeed, the population $P(\mathbf{x},t) \equiv P(x_1, x_1+m_x, t)$ is invariant under a translation along the lattice and it can be expanded as a Bloch wave as

$$P(x_1, x_1 + m_x, t) = \frac{1}{N}\sum_q P_q(m_x, t)e^{iq(x_1+m_x/2)} \tag{27}$$

The total momentum q, which takes N values in the first Brillouin zone of the lattice, is associated to the diffusion of the center of mass of the two polarons. The resulting population $P_q(m_x,t)$ refers to the degree of freedom m_x that characterizes the distance between the two polarons. It varies from 0 to $(N-1)/2$ in order to recover the dimension $N(N+1)/2$ of the two-polaron subspace. Since q is a good quantum number, the Pauli master equation can be solved for each q value. It is expressed as

$$\frac{\partial P_q(m,t)}{\partial t} = -\sum_{m'} D_q(m,m')P_q(m',t) \tag{28}$$

where the non vanishing elements of the diffusion matrix D_q are defined as

$$\begin{aligned} D_q(m,m) \quad &= 2\sum_{\delta=\pm1} W_{m\to m+\delta} \\ D_q(m,m\pm1) &= -2\cos(q/2)W_{m\pm1\to m} \end{aligned} \tag{29}$$

Eq.(28) shows that the diffusion of the two polarons is governed by the diffusion matrix D_q which describes both the purely incoherent processes and dephasing limited coherent motion. For each q value, it is a non hermitian real matrix whose diagonalization leads to $(N+1)/2$ real eigenvalues $\lambda_\sigma(q)$ and eigenvectors $\Pi_{q\sigma}(m)$ labeled by the index σ. Form Eq.(28) and since the two polarons are initially excited on the site

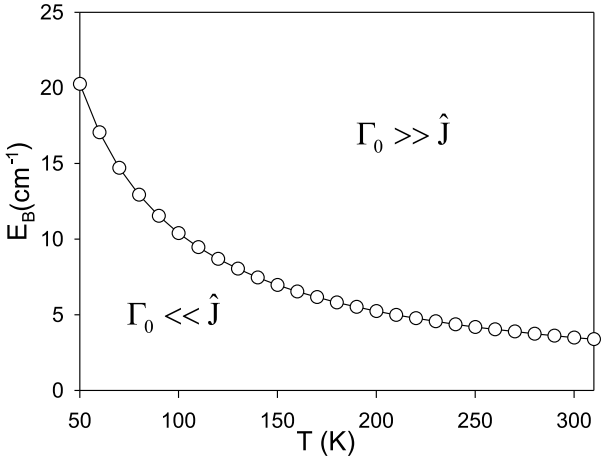

Figure 2. Critical curve in the parameter space which defines the domain of validity of the Pauli master equation (see the text).

$n = x_0$, $P_q(m,t)$ is thus expressed in terms of the characteristics of the diffusion matrix as

$$P_q(m,t) = \sum_{\sigma} \Pi_{q\sigma}(m)\Pi^*_{q\sigma}(0)e^{iqx_0 - \lambda_\sigma(q)t} \tag{30}$$

As shown in Eq.(30), the eigenvalues of the diffusion matrix represent the damping rates of the hydrodynamics modes describing the energy diffusion mediated by the two polarons.

Therefore, as illustrated in the next section, the knowledge of the population $P_q(m,t)$ allows us to define the relevant observables required to characterize the vibrational energy flow. For instance, it gives a complete understanding of the polaron inter-distance kinetic through the definition of the corresponding distribution. This distribution, defined as $\rho_m(t) = P_{q=0}(m,t)$, represents the probability to observe two polarons on the sites x and $x+m$, whatever the position of their center of mass. In addition, it yields the vibron density as

$$g_n(t) = \frac{2}{N}\sum_{qm} \cos(qm/2)P_q(m,t)e^{iqn} \tag{31}$$

This expression allows us to determine the corresponding mean square displacement $\Delta n^2(t) = \langle n^2(t)\rangle - \langle n(t)\rangle^2$ whose time evolution is essential to evaluate the energy diffusion coefficient.

6. Numerical results

In this section, the previous formalism is applied to study the vibrational energy diffusion along a 1D lattice of hydrogen bounded peptide units. To proceed, the parameters W^i, W^c and Γ, required to build the diffusion matrix D_q, are first

evaluated. These calculations are presented in Appendix A. Then, D_q is diagonalized and the corresponding eigenvalues and eigenvectors are used to compute the different observables. These calculations are carried out by using typical values for the relevant parameters. The bare hopping constant is fixed to $J = 8$ cm^{-1} [22, 11] and the intramolecular anharmonicity is $A = 8.0$ cm^{-1} [13]. The phonon cutoff frequency is equal to $\Omega_c = 100$ cm^{-1} and the small polaron binding energy E_B is assumed to range between 0 and 20 cm^{-1}.

Before analyzing the behavior of the transition rates, let us first consider the domain of validity of the Pauli master equation Eq.(24). Within this model, the coherent two-polaron dynamics is neglected and only incoherent processes are taken into account. To be valid, this assumption requires that dephasing occurs over a timescale shorter than the typical time needs to create coherences. As shown in Appendix A, the dephasing constant is about $\Gamma_0 = 128 E_B J^2 k_B T/\Omega_c^3$ (see Eq.(A.8)) whereas the effective hopping constant $\hat{J}$ (Eq.(7)) specifies the timescale for the occurrence of the coherences. Therefore, the model is valid when $\Gamma_0 >> \hat{J}$. As illustrated in Fig. 2, the equation $\Gamma_0 = \hat{J}$ defines a critical curve in the space of the parameters which discriminates between a valid domain (above the curve) and non valid domain (below the curve). It clearly shows that at biological temperature ($T > 300K$) the master equation can be used providing that $E_B > 3.5$ cm^{-1}. Note that below the critical curve the dynamics is governed by the quantum kinetic equation Eq.(18) in which the coherent effects are expected to play a key role in the short time limit, only.

The E_B dependence of both the incoherent and coherent rates are displayed in Figs. 3 for $T = 300$ K. Fig. 3a characterizes the transition between the configurations $m = 0$ (two polarons on the same site) and $m = 1$ (two polarons onto nearest neighbor sites). Both $W^i_{0\to 1}$ (full line) and $W^i_{1\to 0}$ (long dashed line) increase linearly with E_B. Although the two rates are almost identical for small E_B values, the difference between them increases with E_B. By contrast, $W^c_{0\to 1}$ (short dashed line) exhibits two regimes. It first increases for small E_B values to reach a maximum equal to 2.43 cm^{-1} when $E_B = 3$ cm^{-1}. In that case it is greater than the two previous incoherent rates. Then, for greater E_B values, the coherent rate becomes smaller than the incoherent rates and it decreases to finally vanishes.

The rates connected to the transition between the configurations $m = 1$ and $m = 2$ are shown in Fig. 3b. As previously, $W^i_{1\to 2}$ and $W^i_{2\to 1}$ increase linearly with E_B without exhibiting a significant difference. By contrast, $W^c_{1\to 2}$ shows a divergence when E_B tends to zero. It is rather important for small E_B values and it is greater than the incoherent rates providing that $E_B < 6.25$ cm^{-1}. Note that similar features are observed for the transition between the configurations $m = 2$ and $m = 3$ (not drawn).

As shown in Fig. 4 for $T = 300$ K, the full rate $W = W^c + W^i$ exhibits two distinct behaviors depending on both the nature of the transition and the strength of the polaron-phonon coupling. For small E_B values, $W_{0\to 1}$ (circles) is rather weak although it slightly increases with E_B. By contrast, $W_{1\to 2}$ (triangles) and $W_{2\to 3}$ (squares) diverge when E_B tends to zero but decrease when E_B increases. Note that in that regime the asymmetry

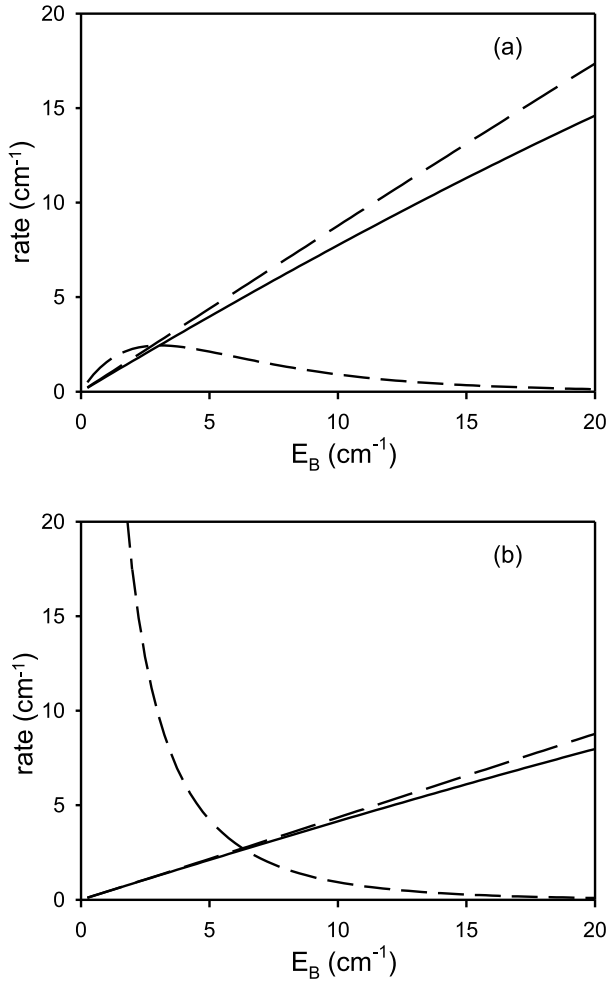

Figure 3. Transition rates $W^i_{m\to m+1}$ (full line), $W^i_{m+1\to m}$ (long dashed line) and $W^c_{m\to m+1}$ (short dashed line) for (a) $m = 0$ and (b) $m = 1$. The temperature is $T = 300$ K.

is rather small. By contrast, when E_B is typically greater than 5 cm^{-1} a new regime takes place. Indeed, $W_{0\to 1}$, which still increases with E_B, becomes the dominant rate. In that case $W_{1\to 2}$ and $W_{2\to 3}$ increase with E_B according to a linear law. Although the asymmetry is now more significant, it only affects the transition between $m = 0$ and $m = 1$.

These features are summarized in Figs. 5 which displays the different rates for $E_B = 5$ cm^{-1} (Fig. 5a) and $E_B = 15$ cm^{-1} (Fig. 5b). For each m value, the figures show $W^i_{m\to m+1}$ (full circles), $W^i_{m+1\to m}$ (open circles), $W^c_{m\to m+1} = W^c_{m+1\to m}$ (triangles), $W_{m\to m+1}$ (full squares) and $W_{m+1\to m}$ (open squares). When $E_B = 5$ cm^{-1}, the smallest rates, which describe the transition between $m = 0$ and $m = 1$, are dominated by their incoherent contributions. By contrast, the transition between sites involving large m values is characterized by a strong rate whose main contribution is the coherent one.

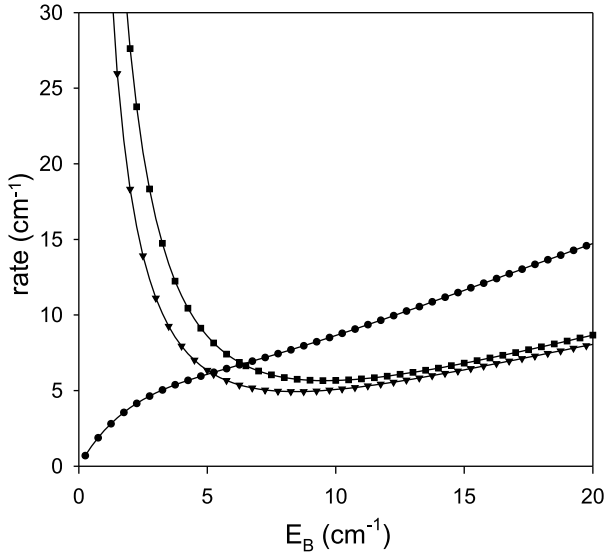

Figure 4. Transition rates $W_{0\to1}$ (circles), $W_{1\to2}$ (triangles) and $W_{2\to3}$ (squares) for $T = 300$ K.

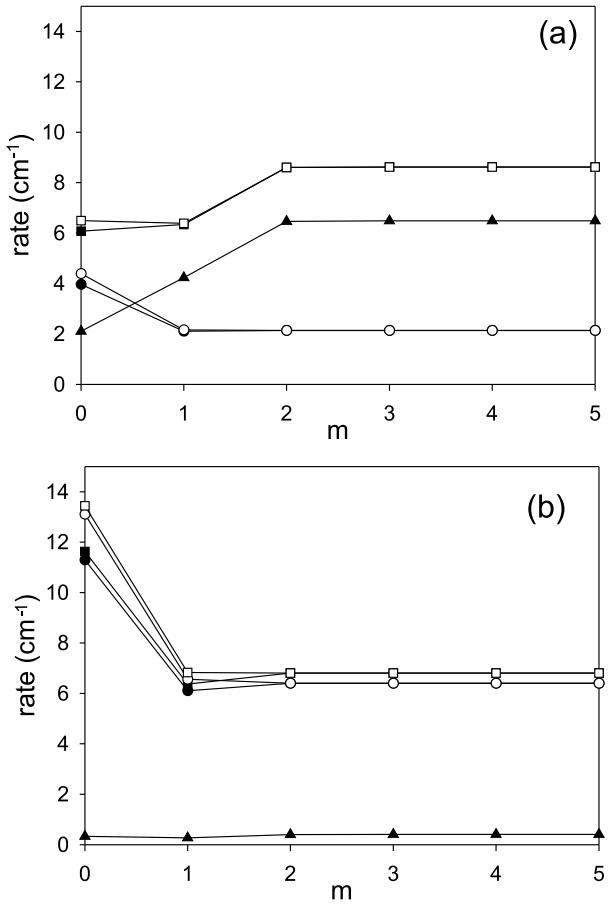

Figure 5. Transition rates $W^i_{m\to m+1}$ (full circles), $W^i_{m+1\to m}$ (open circles), $W^c_{m\to m+1} = W^c_{m+1\to m}$ (triangles), $W_{m\to m+1}$ (full squares) and $W_{m+1\to m}$ (open squares) for (a) $E_B = 5$ cm^{-1} and (b) $E_B = 15$ cm^{-1}. The temperature is $T = 300$ K.

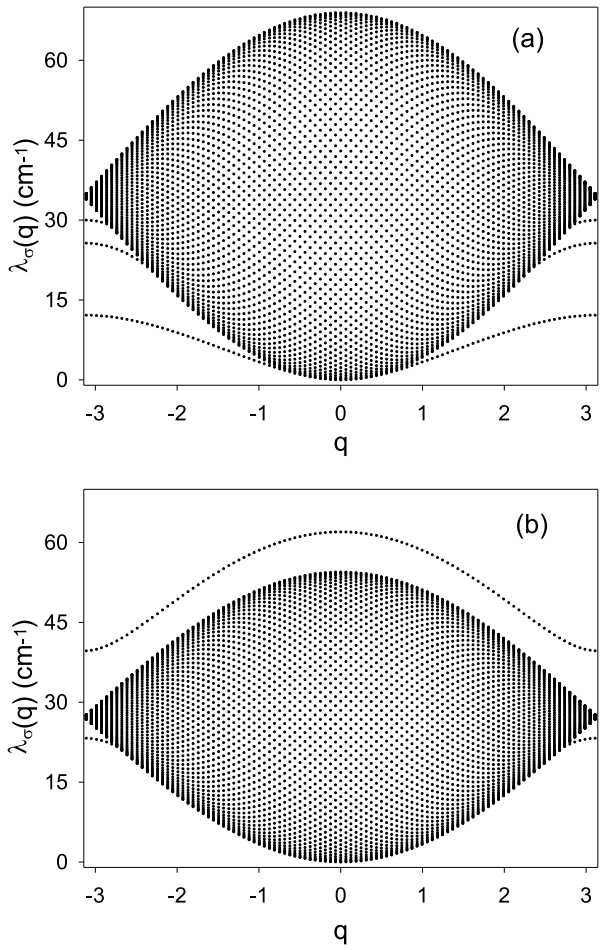

Figure 6. hydrodynamics modes $\lambda_\sigma(q)$ for (a) $E_B = 5$ cm^{-1} and (b) $E_B = 15$ cm^{-1}.

When $E_B = 15$ cm^{-1}, $W_{0\to1}$ and $W_{1\to0}$ appear about two times greater than all the other rates. In that case, the coherent contributions are negligible so that the different rates mainly involve their incoherent parts.

As shown in Figs. 6, the knowledge of the transition rates allows to evaluate the eigenvalues of the diffusion matrix. They are drawn in the first Brillouin zone of the lattice for two typical values of the small polaron binding energy, $E_B = 5$ cm^{-1} (Fig. 6a) and $E_B = 15$ cm^{-1} (Fig. 6b), and for $T = 300$ K. Whatever E_B, the figures clearly show the occurrence of a continuum. The study of the corresponding eigenstates reveals that it contains the modes associated to the diffusion of two independent polarons. Its bandwidth ranges between zero and a maximum value equal to 69 cm^{-1} for $E_B = 5$ cm^{-1} and to 54 cm^{-1} for $E_B = 15$ cm^{-1}.

When $E_B = 5$ cm^{-1}, the spectrum exhibits three specific modes located below the continuum. The analysis of their eigenvectors shows that they correspond to two-polaron hydrodynamics bound modes (TPHBM) in which the two polarons, trapped

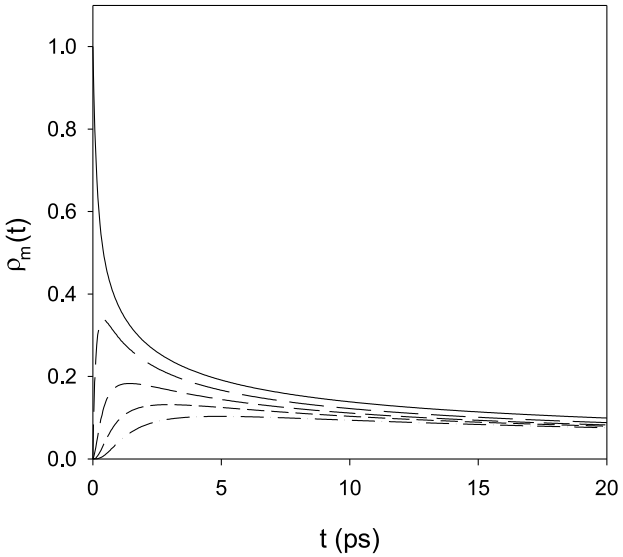

Figure 7. Time evolution of the distribution of the inter-distance between the two polarons for $E_B = 10$ cm^{-1} and $T = 300$ K. $\rho_0(t)$ (full line), $\rho_1(t)$ (long dashed line), $\rho_2(t)$ (medium dashed line), $\rho_3(t)$ (short dashed line), $\rho_4(t)$ (dash dotted line)

close to each other, behave as a single particle diffusing along the lattice. The TPHBM connected to the smallest damping rate characterize two polarons trapped on the same site. They are located below the continuum over the entire Brillouin zone and their damping rate tends to zero when the wave vector q tends to zero. However, the localized nature of the inter-distance between the two polarons strongly decreases when q tends to zero. It finally disappears at the center of the Brillouin zone where the TPHBM clearly refer to two independent polarons. The two other TPHBM occur above a critical value of the wave vector and they correspond to the trapping of the two polarons in the configurations $m = 1$ and $m = 2$, respectively. By contrast, when $E_B = 15$ cm^{-1}, the spectrum shows two TPHBM. The modes located below the continuum correspond to two polarons trapped on the same site. As previously, the bond between the two polarons increases when q tends to zero so that the two polarons appear independent in the vicinity of the center of the Brillouin zone. This is no longer the case for the TPHBM lying above the continuum in which the two polarons are trapped close to each other whatever the value of the wave vector.

The time evolution of the distribution of the inter-distance between the two polarons is illustrated in Fig. 7. For $E_B = 10$ cm^{-1} and $T = 300$ K, the figure shows that the probability distribution exhibits two regimes. In the short time limit, i.e. over a timescale of about 1 ps, $\rho_0(t)$ decreases exponentially whereas the remaining probabilities connected to small m values increase. For instance, $\rho_1(t)$ and $\rho_2(t)$ reach a maximum value equal to 0.34 ($t = 0.4$ ps) and 0.18 ($t = 1.44$ ps), respectively. Such a behavior reveals that a fast energy transfer takes place between the different basis vectors. Therefore, starting with two quanta on the same site ($m = 0$), the bond between the two polarons is rapidly broken due to fast transitions between the

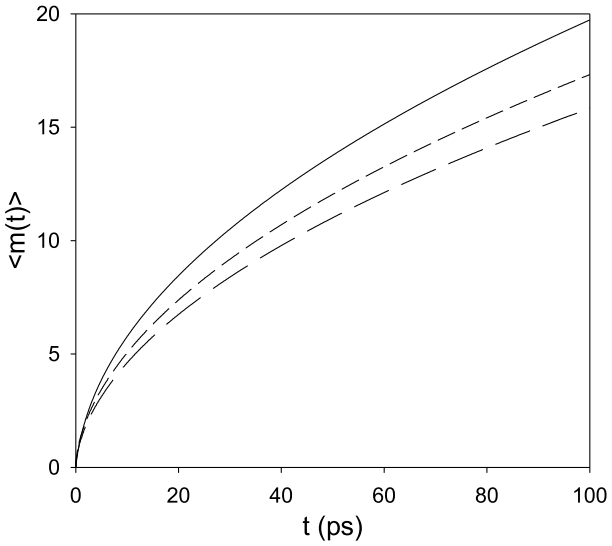

Figure 8. Time evolution of the average inter-distance for $T = 300$ K and $E_B = 5$ (full line), 10 (long dashed line) and 15 (short dashed line) cm^{-1}.

configurations $m = 0$ and $m = 1$. Then, in the long time limit the probability $\rho_0(t)$ slowly decreases according to the power law $t^{-1/2}$. In addition, we observe the propagation of the excitation of the probabilities connected to the large m values. Such a behavior characterizes a diffusive motion of the inter-distance which clearly indicates that the two polarons tend to diffusive independently. Note that a similar behavior is observed for other E_B values but over a different timescale.

Such features are corroborated by the behavior of the average value of the inter-distance between the two polarons displayed in Fig. 8 for for $T = 300$ K and $E_B = 5$ (full line), 10 (long dashed line) and 15 (short dashed line) cm^{-1}. Indeed, whatever the strength of the polaron-phonon coupling, the average inter-distance $< m(t) >$ increases with time which indicates that the two polarons tend to separate. A numerical analysis of the data reveals that $< m(t) >$ typically scales as t^{α}, where $\alpha = 0.53$. This power law, developed whatever the value of E_B, is very close to a square root time dependence in a good agreement with a standard diffusion theory. In fact, the discrepancy with the square root law is observed in the short time limit, only, which results in a small modification of the α value.

Finally, the time evolution of the mean square displacement $\Delta n^2(t)$ connected to the vibron density is shown in Fig. 9 for $E_B = 5$ (full line), 10 (long dashed line) and 15 (short dashed line) cm^{-1}. The temperature is fixed to $T = 300$ K. In the short time limit, $\Delta n^2(t)$ scales as $t^{1.2}$ for $E_B = 5$ cm^{-1} whereas it is almost proportional to t for both $E_B = 10$ cm^{-1} and $E_B = 15$ cm^{-1}. As a consequence, although for $E_B = 5$ cm^{-1} $\Delta n^2(t)$ exhibits the smallest value, it increases more rapidly to finally becomes dominant

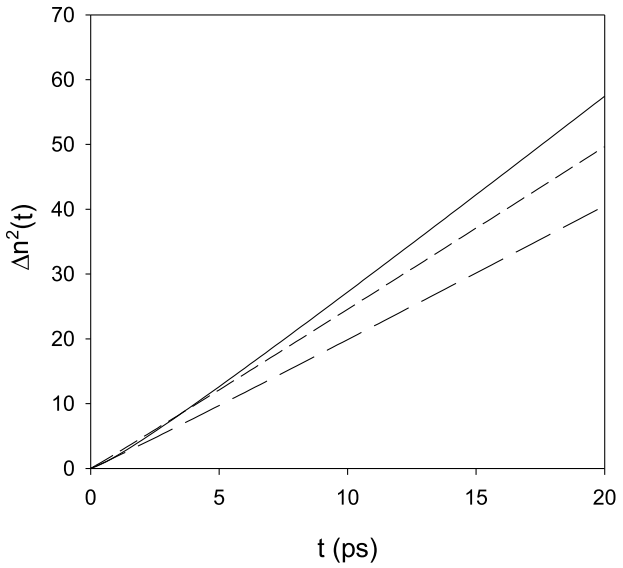

Figure 9. Time evolution of the mean square displacement $\Delta n^2(t)$ for$T = 300$ K and $E_B = 5$ (full line), 10 (long dashed line) and 15 (short dashed line) cm^{-1}.

for a time t greater than 5 ps. In that case, i.e. when t is typically greater than a few picoseconds, $\Delta n^2(t)$ clearly shows a linear dependence with respect to time whatever the value of the polaron-phonon coupling. In other words, in the long time limit, the mean square displacement scales as $\Delta n^2(t) = 2Dt$, where D denotes the energy diffusion coefficient.

As illustrated in Fig. 10 for $T = 200$ K (open circles) and $T = 300$ K (full circles), the diffusion coefficient exhibits a strong E_B dependence. For a rather weak polaron-phonon coupling, the diffusion coefficient decreases with both E_B and the temperature. For instance, for $E_B = 5$ cm^{-1}, it is equal to $D = 13$ cm^{-1} for $T = 200$ K but reduces to $D = 8$ cm^{-1} for $T = 300$ K. It thus reaches a minimum value of about $D = 5.3$ cm^{-1} which occurs for $E_B \approx 14$ cm^{-1} when $T = 200$ K and for $E_B \approx 9$ cm^{-1} when $T = 300$ K. By contrast, for a strong polaron-phonon coupling, the diffusion coefficient increases with E_B, according to a linear law, as well as with the temperature. For instance, for $E_B = 20$ cm^{-1}, it is equal to $D = 6$ cm^{-1} when $T = 200$ K and reaches $D = 8.5$ cm^{-1} when $T = 300$ K.

7. Discussion and Conclusion

The numerical results reveals that, at biological temperature, the polaron-phonon coupling is sufficiently strong to prevent any coherent effect so that TPBS do not play a significant role in the vibrational energy transfer. Indeed, the initial creation of two polarons on a single site mainly excites the TPBS-I band which describes a pair of polarons located on the same amide-I mode [13]. When the coupling with the phonons is disregarded, the coherent energy transfer accounts for the delocalization of

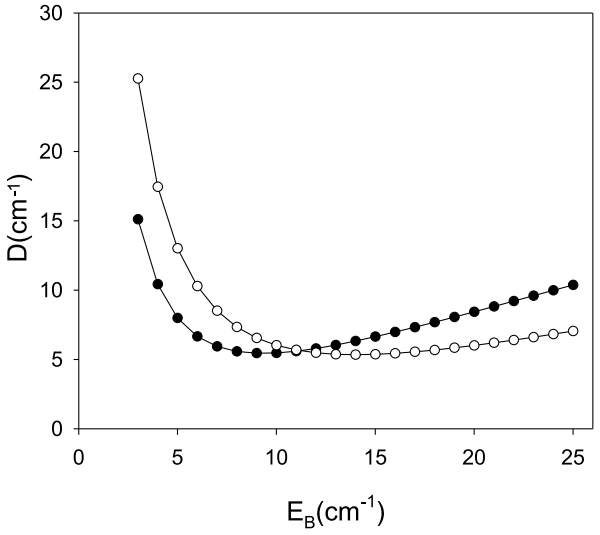

Figure 10. Diffusion coefficient vs E_B for $T = 300$ K (full circle) and $T = 200$ K (open circles).

the pair which behaves as a single particle propagating along the lattice. When the polaron-phonon interaction is turned on, this behavior disappears since the coupling is responsible for the occurrence of transitions between the difference two-polaron eigenstates. As a result, the bond between the two polarons is broken after a few picoseconds and an incoherent energy transport takes place mediated by two independent polarons.

This result originates in the polaron-phonon interaction which induces random fluctuations in the polaron hopping constant and favors the occurrence of two fundamental mechanisms. First, a polaron is able to perform a hop between two nearest neighbor lattice sites by absorbing or emitting a phonon. Such a mechanism, which corresponds to a transition between the configurations m and $m \pm 1$, is described by the incoherent rate $W^i_{m\to m\pm 1}$. Then, the fluctuations of the hopping constant break the coherent polaron dynamics leading to additional transitions. Basically, starting with two polarons separated by m sites, the Hamiltonian favors the coherent superimposition of the configurations m and $m \pm 1$. However, during the time evolution of the full system, the coupling with the phonons yields random fluctuations of each phase which destroy the coherence of the superimposition. The polarons are thus described by a statistical mixture of the configurations m and $m \pm 1$ which can be viewed as the consequence of an incoherent hop. Nevertheless, since this transition originates in the interplay between the coherent motion and the dephasing, it is called a coherent transition and is characterized by the coherent rate $W^c_{m\to m\pm 1}$.

The behavior of the rates strongly depends on the nature of the transition. When the two polarons lye far apart, i.e. for large m values, the energy difference between two configurations m and $m \pm 1$ vanishes. The corresponding incoherent and coherent rates, denoted W^i_0 and W^c_0 respectively, are defined in Eq.(A.8). W^i_0 increases linearly with

E_B whereas W_0^c decreases due to the E_B dependence of both the dephasing constant Γ_0 and the coupling constant $S(T)$ (see Eq.(7)). As a consequence, the coherent rate dominates for small E_B values whereas the incoherent rate becomes larger for strong E_B values.

When the two polarons are close to each other a strong modification of the transition rates occurs due to the anharmonic nature of the polaron dynamics. When two polarons are on the same site ($m = 0$), both the intramolecular anharmonicity and the vibron-phonon coupling favor a redshift of the corresponding energy equal to $\epsilon_0 = 2\hat{\omega}_0 - 2(A + E_B)$. In the same way, when two polarons are located onto nearest neighbor sites ($m = 1$), the overlap between their virtual cloud of phonons yield a redshift of the energy equal to $\epsilon_1 = 2\hat{\omega}_0 - E_B$. Therefore, the incoherent transition from $m = 0$ to $m = 1$, which requires the absorption of a phonon whose energy is equal to $\epsilon_1 - \epsilon_0 = 2A + E_B$, is less probable than the incoherent transition form $m = 1$ to $m = 0$. An asymmetry in the transition rates occurs and increases with the energy difference, i.e. with E_B. Nevertheless, at biological temperature, such feature does not play a significant role due to the rather small anharmonicity of the amide-I mode. Similarly, the behavior of the coherent rate $W^c_{0\to1}$ originates in the competition between the dephasing constant Γ_{01} and the energy difference $\epsilon_1 - \epsilon_0$. For small E_B values, $\Gamma_{01} << \epsilon_1 - \epsilon_0$ so that $W^c_{0\to1}$ scales as Γ_{01}/A. It thus vanishes when E_B tends to zero since Γ_{01} is proportional to small polaron binding energy (see Appendix A). By contrast, for greater E_B values, $\Gamma_{01} >> \epsilon_1 - \epsilon_0$ so that $W^c_{0\to1} \propto 1/\Gamma_{01}$. These results allows us to understand the different numerical observations such as the behavior of the full rate $W_{0\to1}$ displayed in Fig. 4. For small E_B value, this rate clearly involves both the coherent and the incoherent rates whereas only the incoherent rate contributes significantly for strong E_B values.

The E_B dependence of the incoherent rates $W^i_{1\to2}$ and $W^i_{2\to1}$ is rather similar to that of the previous incoherent rates although the asymmetric effect has been drastically reduced because the energy difference between the configurations $m = 1$ and $m = 2$ is $\epsilon_2 - \epsilon_1 = E_B$. As previously, the competition between Γ_{12} and $\epsilon_2 - \epsilon_1$ governs the behavior of $W^c_{1\to2}$. Since both Γ_{12} and $\epsilon_2 - \epsilon_1$ are proportional to E_B, the coherent rate scales as $W^c_{1\to2} \propto 1/E_B$ and thus diverges for small E_B values (see Fig. 3b). As a consequence, the full rate $W_{1\to2}$ and $W_{2\to1}$ are clearly dominated by their coherent part for small E_B values, as observed in Fig. 4, but the incoherent rates become dominant for large E_B values.

The nature of the rates clearly discriminates between transitions involving configurations with small m values and transitions connected to configurations with large m values. In other words, the spectrum of the diffusion matrix exhibits two kinds of hydrodynamics modes. The modes describing two independent polarons diffusing along the lattice form a continuum in which the damping rates range between zero and a maximum value. To understand this feature, let us consider the solution of the Pauli master equation Eq.(28) for large m values by disregarding the influence of the

configurations close to $m = 0$. In that case, the Pauli master equation is written as

$$\frac{\partial P_q(m,t)}{\partial t} = 2\cos(\frac{q}{2})W_0[P_q(m+1,t) + P_q(m-1,t)] - 4W_0P_q(m,t) \quad (32)$$

where $W_0 = W_0^i + W_0^c$ is the full rate for a transition between m and $m \pm 1$ for large m value (see appendix A). The fundamental solution of Eq.(32) is a plane wave $P_q(m,t) \approx \exp(iKm - \lambda_K(q)t)$ which defines the hydrodynamics modes whose dispersion relation is expressed as

$$\lambda_K(q) = 4W_0(1 - \cos(q/2)\cos(K)) \quad (33)$$

Note that the real modes are superimpositions of progressive and regressive plane waves due to the existence of the boundary $m = 0$. A given hydrodynamics mode, whose damping rate is equal to $\lambda_K(q)$, defines two independent diffusive modes with wave vectors $k_1 = q/2 + K$ and $k_2 = q/2 - K$ and damping rates $\lambda_{k_1} = 2W_0(1 - \cos(k_1))$ and $\lambda_{k_2} = 2W_0(1 - \cos(k_2))$. These two modes describe the incoherent motion of two independent polarons and will be called two-polaron hydrodynamics free modes (TPHFM). Therefore, the TPHFM belong to a continuum which extends from zero to $8W_0$. For $E_B = 5$ and 15 cm^{-1}, $W_0 = 8.62$ and 6.81 cm^{-1}, respectively, so that the maximum damping rate is equal to 68.9 and 54.5 cm^{-1}, in a perfect agreement with the numerical results shown in Fig. 6.

In addition to the TPHFM, the singularity of the transition rates in the vicinity of the configuration $m = 0$ favors the occurrence of specific modes located below or above the continuum. In fact, similarly to the occurrence of bound states in a nonlinear lattice [13], these modes are characterized by a complex value of the wave vector $K = K' + i\kappa$, with $K' = 0$ or π. As a result, the corresponding probability behaves as $P_q(m,t) \approx \exp(-\kappa m)$ and refers to hydrodynamics modes in which the separating distance between the two polarons is localized. For that reason, these modes have been called two-polaron hydrodynamics bound modes (TPHBM) in the previous section. The TPHBM thus characterize two trapped polarons diffusing along the lattice as a single particle. Nevertheless, although the initial creation of two polarons on the same site mainly excites such modes, our results reveal that TPHBM do not play a significant role in the long time behavior of the energy flow. Indeed, the TPHBM located above the continuum ($K' = \pi$) exhibit a rather important damping rate typically of about $4W_0(1 + \cosh(\kappa))$. Since this value is greater than or about to $8W_0$, the TPHBM govern the energy transfer over a very short timescale and finally disappear after a few picoseconds. In the same way, the TPHBM located below the continuum ($K' = 0$) are characterized by a damping rate $4W_0(1 - \cosh(\kappa))$. For positive κ values, they have a non vanishing damping rate and play a key role in the short time limit, only. In fact, the long time behavior is mainly governed by the TPHBM localed close to the center of the Brillouin zone which are characterized by a very small κ value. In that case the localized nature of the polaron inter-distance disappears so that the TPHBM mainly describe the diffusive motion of two independent polarons.

The main consequence is that the vibrational energy flow in a 1D lattice of hydrogen bounded peptide units is mediated by the incoherent motion of two independent

polarons. Therefore, in the long time limit, this motion corresponds to a diffusive motion carried by the long wavelength TPHFM and characterized by the energy diffusion coefficient D. As mentioned in the previous section, this coefficient describes the long time behavior of the mean square displacement $\langle \Delta n^2(t) \rangle$ connected to the vibron density expected to scales as $\langle \Delta n^2(t) \rangle \approx 2Dt$. To evaluate this coefficient, let us mention that the mean square displacement can be expressed as

$$\langle \Delta n^2(t) \rangle = \langle \Delta X_{cm}^2(t) \rangle + \frac{\langle m^2(t) \rangle}{4} \tag{34}$$

where $X_{cm} = (x_1 + x_2)/2$ is the position of the center of mass of the two polarons.

In the long time limit, the dynamics of the polaron inter-distance m is governed by the long wavelength disturbances of the zero wave vector TPHFM ($q = 0$). These modes are characterized by the dispersion relation $\lambda_K(q = 0) \approx 2W_0K^2$ (see Eq.(33)). Therefore, by using the standard diffusion theory within the continuum limit, it is straightforward to shown that the distribution of the inter-distance between the two polarons is approximated as

$$\rho_m(t) \approx \frac{1}{\sqrt{2\pi W_0 t}} \exp\left(\frac{-m^2}{8W_0 t}\right) \tag{35}$$

Since m is positive, its average value does not vanish and reduces to $\langle m(t) \rangle = \sqrt{8W_0 t/\pi}$, in a rather good agreement with the results displayed in Fig. 8. In addition, the associated second moment behaves as $\langle m^2(t) \rangle = 4W_0 t$ which allows us to defined the diffusion coefficient $D_m = 2W_0$ connected to the polaron inter-distance.

In the same way, the moments of the center of mass distribution can be expressed in terms of the population $P_q(m, t)$ as

$$\langle X_{cm}^{\alpha}(t) \rangle = i^{\alpha} \sum_m \left(\frac{d^{\alpha}}{dq^{\alpha}} P_q(m, t) \right)_{q=0} \tag{36}$$

Since the diffusion is mainly governed by the TPHFM , only the mode $K = 0$ whose damping rate vanishes when q tends to zero contributes significantly to the evolution of the mean square displacement $\langle \Delta X_{cm}^2(t) \rangle$. Therefore, by inserting Eq.(30) into Eq.(36), an after performing simple algebraic manipulations, it is straightforward to show that in the long time limit $\langle \Delta X_{cm}^2(t) \rangle$ is written as

$$\langle \Delta X_{cm}^2(t) \rangle = \left(\frac{d^2 \lambda_{K=0}(q)}{dq^2} \right)_{q=0} t \tag{37}$$

The mean square displacement thus scales as $\langle \Delta X_{cm}^2(t) \rangle = 2D_{cm}t$, where the center of mass diffusion coefficient is expressed as $D_{cm} = W_0/2$.

Finally, from Eq.(34), the energy diffusion coefficient is defined as $D = W_0$. In terms of the relevant parameters of the problem, it is expressed as (see Eq.(A.8))

$$D = \frac{32 E_B J^2 k_B T}{\Omega_c^3} + \frac{\Omega_c^3 \hat{J}^2}{64 E_B J^2 k_B T} \tag{38}$$

As shown in Eq.(38), the energy diffusion coefficient is the sum of two contributions. Indeed, the first term in the right-hand-side of Eq.(38) characterizes incoherent

transitions. It increases with both the small polaron binding energy and the temperature, as explained in the description of the corresponding rates. By contrast, the second term in the right-hand-side of Eq.(38) accounts for coherent transitions. It thus decreases with both the polaron-phonon coupling strength and the temperature. Therefore, for small E_B values or in the low temperature limit, the diffusive motion of the polarons is mainly governed by coherent transitions connected to the limitation of the coherent motion by dephasing. By contrast, for a strong polaron-phonon coupling or in the high temperature limit, incoherent transitions dominate the diffusion. Nevertheless, in both cases, the two polarons diffuse independently so that D is equal to the energy diffusion coefficient connected to the motion of a single polaron. The polaron-polaron interaction does not affect the long time behavior of the energy flow so that the diffusion is insensitive to the nonlinear nature of the lattice.

Appendix A. Calculation of the transition rates and of the dephasing constants

For the amide-I mode, the small polaron binding energy E_B is about one order of magnitude smaller than the phonon cutoff frequency so that the dressing operator Eq.(5) can be linearized [14]. As a consequence, the coupling term $V_{n,n'}$ (see Eq.(8)) between the polarons and the remaining phonons is expressed as

$$V_{n,n'} \approx \sum_q \frac{i\Delta_0 J}{\sqrt{N}\Omega_c} \frac{\sin(q)}{|\sin(q/2)|^{3/2}} [(e^{-iqn} - e^{-iqn'})a_q^\dagger + H.c.] \tag{A.1}$$

By inserting Eq.(A.1) into Eq.(17), the correlation function $C(t)$ is written as

$$C(t) = \frac{8E_B J^2}{N\Omega_c} \sum_q \cos^2(q/2)|\sin(q)|[n_q e^{i\Omega_q t} + (n_q+1)e^{-i\Omega_q t}] \tag{A.2}$$

where $n_q = n_B(\Omega_q) = 1/(\exp(\Omega_q/k_BT) - 1)$ is the Bose number.

As explained in the text, it has been assumed that over a timescale of about the phonon bath correlation time, the polaron does not move significantly. Therefore, the diagonal element of the polaron evolution operator can be approximated as

$$G(m,t) = \exp(-i\epsilon_m t) \tag{A.3}$$

where ϵ_m is the self-energy of a site $|\mathbf{x}) \equiv |x, x+m)$. As illustrated in Fig. 1, the self-energy only depends on the separating distance between the two polarons as

$$\epsilon_m = \begin{cases} 2\hat{\omega}_0 - 2(A+E_B) & \text{if } m = 0 \\ 2\hat{\omega}_0 - E_B & \text{if } m = 1 \\ 2\hat{\omega}_0 & \text{if } m > 1 \end{cases} \tag{A.4}$$

Therefore, by inserting Eqs.(A.2) and (A.3) into the definition of the incoherent rate Eq.(21) we obtain :

$$W^i_{m\to m\pm1} = \frac{32E_B J^2}{\Omega_c^2}(1+\delta_{m,0})(1+\delta_{m',0})F(\epsilon_{m\pm1} - \epsilon_m) \tag{A.5}$$

where

$$F(\omega) = \begin{cases} \frac{\omega}{\Omega_c}\sqrt{1-(\frac{\omega}{\Omega_c})^2}n_B(\omega) & \text{if } \omega \geq 0 \\ -\frac{\omega}{\Omega_c}\sqrt{1-(\frac{\omega}{\Omega_c})^2}(n_B(-\omega)+1) & \text{if } \omega < 0 \end{cases} \tag{A.6}$$

with $F(0) = k_B T/\Omega_c$.

At this step, a similar procedure can be used to evaluate the dephasing constant defined in Eq.(20). After some straightforward calculations, it is expressed in terms of the incoherent rates as

$$\Gamma_{m_x,m_y} = \sum_{\delta=\pm 1} W^i_{m_x \to m_x+\delta} \frac{F(\epsilon_{m_x+\delta} - \epsilon_{m_y})}{F(\epsilon_{m_x+\delta} - \epsilon_{m_x})} + W^i_{m_y \to m_y+\delta} \frac{F(\epsilon_{m_y+\delta} - \epsilon_{m_x})}{F(\epsilon_{m_y+\delta} - \epsilon_{m_y})} \tag{A.7}$$

Finally, the coherent rates Eq.(25) are easily computed from the knowledge of the dephasing constant.

To illustrate these results, let us define the different parameters connected to the diffusive behavior of two polarons lying far apart ($m >> 0$). In that case, the rates for both incoherent (W_0^i) and coherent (W_0^c) transitions as well as the dephasing constant Γ_0 are defined as

$$\begin{aligned} W_0^i &= \frac{32 E_B J^2 k_B T}{\Omega_c^3} \\ \Gamma_0 &= \frac{128 E_B J^2 k_B T}{\Omega_c^3} \\ W_0^c &= \frac{2\hat{J}^2}{\Gamma_0} \end{aligned} \tag{A.8}$$

References

[1] A. S. Davydov and N. I. Kisluka 1973 Phys. Status Solidi **59** 465; 1976 Zh. Eksp. Teor. Fiz **71** 1090 [1976 Sov. Phys. JETP **44** 571].

[2] A.C. Scott 1992 Phys. Rep. **217** 1 .

[3] P. L. Christiansen and A. C. Scott 1990 *Davydov's Soliton Revisited* (Plenum, New York).

[4] S. Aubry 1997 Physica **D103** 201.

[5] S. Flach and C.R. Willis 1998 Phys. Rep. **295** 181.

[6] R.S. MacKay 2000 Physica **A288** 174.

[7] A. J. Sievers and S. Takeno 1988 Phys. Rev. Lett. **61** 970.

[8] D.W. Brown and Z. Ivic 1989 Phys. Rev. **B40** 9876.

[9] D.W. Brown, K. Lindenberg and X. Wang 1990 *Davydov's Soliton Revisited* ed. P. L. Christiansen and A. C. Scott (Plenum, New York) .

[10] Z. Ivic, D. Kapor, M. Skrinjar and Z. Popovic 1993 Phys. Rev. **B48** 3721.

[11] Z. Ivic, D. Kostic, Z. Przulj and D. Kapor 1997 J. Phys. Condens. Matter **9** 413.

[12] J. Tekic, Z. Ivic, S. Zekovic and Z. Przulj 1999 Phys. Rev. **E60** 821.

[13] V. Pouthier 2003 Phys. Rev. **E68** 021909.

[14] V. Pouthier and C. Falvo 2004 Phys. Rev. **E69** 041906.

[15] C. Falvo and V. Pouthier 2005 J. Chem. Phys. **123** 184709.

[16] C. Falvo and V. Pouthier 2005 J. Chem. Phys. **123** 184710.

[17] V. Pouthier 2006 Physica **D221** 13.
[18] V. Fleuro 2003 Chaos **13** 676.
[19] J.C. Eilbeck 2003 *Some exact results for quantum lattice problems* ed. L. Vasquez, R.S. Mackay and M. P. Zorzano Proc. of the Third Conference Localization and Energy Transfert in Nonlinear Systems (World Scientific, Singapore).
[20] J. C. Kimball, C. Y. Fong and Y. R. Shen 1981 Phys. Rev. **B23** 4946.
[21] F. Bogani, G. Cardini, V. Schettino and P. L. Tasselli 1990 Phys. Rev. **B42** 2307.
[22] A. C. Scott, J. C. Eilbeck and H. Gilhoj 1994 Physica **D78** 194.
[23] L. Proville 2005 Phys. Rev. **B71** 1043306.
[24] J. Edler, R. Pfister, V. Pouthier, C. Falvo and P. Hamm 2004 Phys. Rev. Lett. **93** 106405.
[25] J. Rammer 1998 *Quantum Transport Theory* (Perseus, Massachusetts).
[26] W. Pfluegl, M. A. Palenberg and R. J. Silbey 2000 J. Chem. Phys. **113** 5632.
[27] M. Esposito and P. Gaspard 2005 Phys. Rev. **B71** 214302.
[28] V. Pouthier and J.C. Light 2000 J. Chem. Phys. **113** 1204.
[29] V. Pouthier, J.C. Light and C. Girardet 2001 J. Chem. Phys. **114** 4955.
[30] I. G. Lang and Yu. A. Firsov 1962 Sov. Phys. JETP **16** 1293.
[31] H. Dolderer and M. Wagner 1998 J. Chem. Phys. **108** 261.
[32] S. Mukamel 1995 *Principles of Nonlinear Optical Spectroscopy* (Oxford University Press, Oxford).
[33] R. Zwanzig 1961 Lect. Theoret. Phys. **3** 106; 1964 Physica **30** 1109;1960 J. Chem. Phys. **33** 1338.
[34] H. Mori Prog. 1965 Theoret. Phys. **33** 423; 1965 Prog. Theoret. Phys. **34** 399.